The 2010 IEEE/RSJ International Conference on
Intelligent Robots and Systems
October 18-22, 2010, Taipei, Taiwan

Multi-DOF Model-Based Force Control for Telerobotic Applications

J. Scot Hart and Günter Niemeyer

Abstract— **For a wide range of telerobotic applications, the slave device needs to be a large, powerful, industrial type robot in order to achieve the desired tasks. Due to the large frictional forces within the gearing of such robots, a force-feedback controller is necessary to precisely control the forces the robot applies when manipulating its environment. This paper proves passivity, and therefore guarantees stability, of a model-based force controller in one degree of freedom (DOF) when subject to viscous and Coulomb friction. The controller is then expanded to muli-DOF systems.**

In addition to maintaining the robustness of the 1-DOF controller, the multi-DOF controller provides additional freedom to design the closed loop dynamics of the robot. This freedom allows the control designer the ability to shape and optimize how the system feels from a users perspective. The robustness of the controller is experimentally validated and the freedom to modify the closed loop dynamics is explored using a 2-DOF device.

I. INTRODUCTION

The real strength of telerobotics is the notion that for any possible environment we would like to manipulate, a robot can be built and inserted into that environment providing a portal from which we can explore. In particular, telerobotics really proves beneficial when the environment of interest is at the extreme, be it too small and delicate, too large and heavy, too far away, or just too dangerous for normal unassisted human interaction.

Of particular interest to us is the case when the environment is very large and heavy. For example, space based construction and maintenance requires large industrial type slave robots such as Ranger pictured in Fig. 1. In order to produce the necessary strength to perform the desired tasks, industrial robots typically have a significant amount of gearing within their actuators resulting in large internal frictional forces. Without any compensation, the user can not distinguish between the forces arising from contact with the environment and the internal friction forces in the slave.

In order to achieve precise dexterous manipulation of the remote environment, the user must be able to see through the friction in the system to develop a true understanding of the interaction dynamics between robot and environment. Typically this requires the use of a force-feedback loop using measurements from a force sensor at the end-effector [1] or open-loop compensation based on a friction model [2].

This work was supported by NASA through the Institute for Dexterous Space Robotics

J. Scot Hart is a Senior Robotics Engineer at Hansen Medical, Mountain View, California, USA. He recently received his Ph.D. from Stanford University's department of Mechanical Engineering. hartj@stanford.edu

Günter Niemeyer is a Senior Research Scientist at Willow Garage, Menlo Park, California, USA and a Consulting Professor at Stanford University.

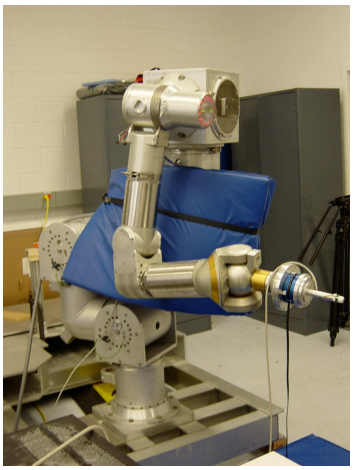

Fig. 1. The University of Maryland Space Systems Lab's Ranger slave robot designed for servicing of satellites in orbit.

Directly feeding the measured force back to the user has proven to be of limited benefit [3], so many control architectures include a local force control loop around the slave robot [4], [5]. In addition to focusing control effort at the source of the friction disturbances, local force control produces cleaner and more ideal closed loop robot dynamics making it easier to design and implement the telerobotic system.

Unfortunately force control loops are notoriously difficult to design. It is well known that force controllers have difficulty maintaining stability when interacting with stiff environments. Since, in the case of telerobotics, the environment is largely unknown it is very important to make sure any force control loops around the slave device are stable for all possible environments. One method to ensure stability is to design the force controller such that the resulting closed loop robot is passive. By maintaining passivity we can be certain that there will not be any energy leaks within the controller that can cause the robot to act uncontrollably regardless of the environment it is in contact with.

Using passivity analysis, studies have shown that force controllers that try to hide some of the robot's inertia are not passive once we account for higher order dynamics such as structural compliance [6]. In response natural admittance control (NAC) was developed as a passive means of force control for autonomous robots [7], [8]. NAC effectively trades off the ability to hide inertial forces for enhanced stability and friction rejection.

Expanding upon NAC, we have introduced a telerobotic model-based force control for 1-DOF systems designed to

passively reject friction forces and maintain a high level of robustness to unmodeled dynamics [9]. When implemented within a bilateral telerobotic system, model-based force control effectively cleans up the slave dynamics such that the user feels like they are interacting with the remote environment through an ideal frictionless robot.

In this paper, we present a passivity analysis for model-based force control showing the resulting system to be passive when subject to both viscous and coulomb friction forces. The model-based control algorithm is then expanded to multiple degree of freedom devices. The resulting muli-DOF algorithm provides the ability to shape the closed loop dynamics of the robot, and therefore the feel of the telerobotic system. The stability of multi-DOF model-based force control is validated experimentally, and the ability to modify the feel of the system is explored.

II. 1-DOF PASSIVITY ANALYSIS

The model-based force control algorithm is extremely robust due to its ability to accommodate the large force spikes that occur upon impact with stiff environments. Traditional force controllers see the force spikes as a large force error causing the controller to produce a large control effort in the opposite direction. Unfortunately, this control effort always lags at least slightly behind the impact force. Combining this lag in the control effort with the hard non-linearity of making and breaking contact the robot motion deteriorates into contact instability.

To avoid contact instability, the model-based force controller uses a model of the robot to provide the controller with information on how the robot will react to the forces seen at the end-effector. In the 1-DOF case, as shown in Fig. 2, the model consist of an ideal frictionless reference mass M_r representing the robot which is subject to both the desired force F_d and measured environmental force F_e.

$$M_r \ddot{x}_m = F_d - F_e \tag{1}$$

Since the model velocity $\dot{x}_m$ represents the ideal velocity of the robot in the absence of internal friction and other disturbance forces, a velocity controller is implemented to make the robot follow the model velocity.

$$F_c = K_v(\dot{x}_m - \dot{x}) \tag{2}$$

The resulting equation of motion for the robot then becomes

$$M\ddot{x} = (F_d - F_e) + (F_c - F_f) \tag{3}$$

where F_f is the internal friction force in the system. Breaking up the forces acting on the robot, $(F_d - F_e) = F_{ext}$ is the net external force acting on the robot and $(F_c - F_f)$ represents the residual disturbance after the force control is applied.

To show passivity of this model reference force controller we must verify the residual disturbance is passive. First we examine the dynamics of F_c. Subtracting (3) from (1) followed by subtracting $M_r\dot{x}$ from both sides of the equation

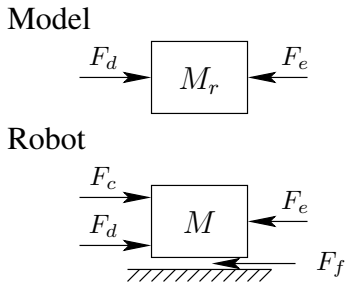

Fig. 2. 1-DOF model and robot

results in the following linear time-invariant (LTI) differential equation for the control force F_c.

$$\frac{M_r}{K_v}\dot{F}_c + F_c = F_f - (M_r - M)\ddot{x} \tag{4}$$

The above expression shows the control force is simply a low-passed version of the internal friction force F_f and an inertial force $(M_r - M)\ddot{x}$ arising from the difference in the model and robot masses.

Assuming the friction forces on the robot consist of viscous and Coulomb friction forces the friction force F_f can be expressed as:

$$F_f = F_{fv} + F_{fc} \quad \text{where}$$
$$F_{fv} = b\dot{x} \quad \text{and} \quad F_{fc} = Csgn(\dot{x}) \tag{5}$$

Since (4) is LTI, superposition holds and the control force can be viewed as the summation of three separate control forces arising to compensate for each type of friction and the inertial force arising from the mass difference.

$$F_c = F_{cv} + F_{cc} + F_{cm} \tag{6}$$

where

$$\frac{M_r}{K_v}\dot{F}_{cv} + F_{cv} = F_{fv} \tag{7}$$
$$\frac{M_r}{K_v}\dot{F}_{cc} + F_{cc} = F_{fc} \tag{8}$$
$$\frac{M_r}{K_v}\dot{F}_{cm} + F_{cm} = -(M_r - M)\ddot{x} \tag{9}$$

Since the control forces are low-pass filtered versions of the friction forces the above expressions can be thought of as disturbance estimators for the friction forces. After applying our estimate of the disturbances the residual friction forces, $F_{fv} - F_{cv}$ and $F_{fc} - F_{cc}$, become high-passed versions of the friction forces.

$$F_{f(v,c)} - F_{c(v,c)} = \left[1 - \frac{K_v}{M_r s + K_v}\right] F_{f(v,c)} = \frac{M_r s}{M_r s + K_v} F_{f(v,c)} \tag{10}$$

Using these expressions combined with (9) the system can now be expressed by the block diagram of fig. 3.

Since the block diagram representation of the closed-loop robot consist of the robot connected in feedback with three systems representing the friction and control forces on the

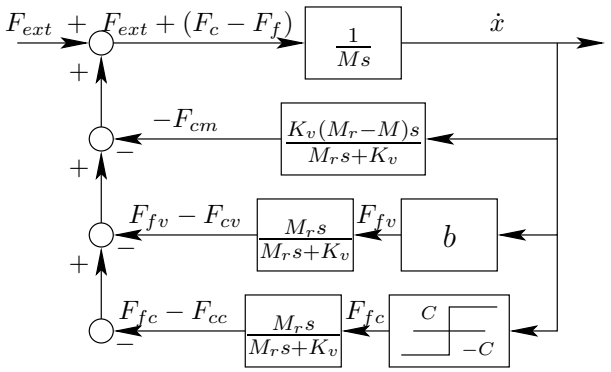

Fig. 3. Block diagram showing passivity of 1-DOF model-based force control.

robot, we need only show the robot and each of the feedback systems is passive to show the entire system is passive.

In the case of LTI systems passivity is equivalent to requiring the transfer function from input to output to be positive real, which is equivalent to requiring the phase of the transfer function to always be between $\pm 90°$. From this we see that the robot and the system representing the viscous friction and its compensation are passive.

$$G_{robot}(s) = \frac{1}{Ms} \tag{11}$$

$$G_{viscous}(s) = b\frac{M_r s}{M_r s + K_v} \tag{12}$$

Furthermore if we stipulate that $M_r \geq M$ the system representing the control force arising from the difference in the model and robot masses is also passive.

$$G_{inertia}(s) = (M_r - M)\frac{K_v s}{M_r s + K_v} \tag{13}$$

This leaves only the system which describes the Coulomb friction and its compensation. Since Coulomb friction is inherently non-linear we explicitly examine the net power flow into the system.

$$\int \dot{x}(F_{fc} - F_{cc})\,\mathrm{d}t \tag{14}$$

For any given non-zero velocity $\dot{x}$ the Coulomb friction force F_{fc} must be either C or $-C$ corresponding to the sign of the velocity. Since F_{cc} is a low-passed version of F_{fc} we can bound F_{cc}.

$$|F_{cc}| \leq C \tag{15}$$

Combining the two forces we see that

$$0 \leq F_{fc} - F_{cc} \leq 2C \quad \text{for} \quad \dot{x} > 0 \tag{16}$$

$$-2C \leq F_{fc} - F_{cc} \leq 0 \quad \text{for} \quad \dot{x} < 0 \tag{17}$$

which implies

$$(F_{fc} - F_{cc})\dot{x} \geq 0 \tag{18}$$

This ensures the integral of (14) is always positive indicating a passive system and therefore completing the analysis showing model-based force control to be passive in 1-DOF.

While friction in general may include other nonlinear terms which have been neglected in the above analysis, we feel confident that viscous and Coulomb friction represent the majority of the disturbance forces. As such, showing passivity with respect to these two friction forces indicates model-based force control will be very robust in practice.

III. MULTI-DOF IMPLEMENTATION

Working in joint space, the model-based force controller can be expanded to multi-DOF robots resulting in the control algorithm depicted in Fig. 4. Here the robot equations of motion are:

$$\boldsymbol{M}(q)\ddot{q} + \boldsymbol{C}(q,\dot{q})\dot{q} = \tau_d + \tau_c - \tau_f - \tau_e \tag{19}$$

Since the reference model needs to capture the inertial behavior of the robot, which changes as it moves across the workspace, the model mass matrix $\boldsymbol{M_r}$ and centripetal and Coriolis matrix $\boldsymbol{C_r}$ must be defined based on the robot's position q and velocity $\dot{q}$.

$$\boldsymbol{M_r}(q)\ddot{q}_m + \boldsymbol{C_r}(q,\dot{q})\dot{q}_m = \tau_d + \tau_e \tag{20}$$

Simulating the model, using the τ_d and τ_e as the inputs, provides the model velocity vector $\dot{q}_m$. This velocity vector represents the ideal joint velocities the robot would have at any given moment based on its position, velocity, and applied external torques if friction forces were not present.

To get the model to follow this ideal velocity vector the control torques are given by:

$$\tau_c = \boldsymbol{K_v}(\dot{q}_m - \dot{q}) \tag{21}$$

where $\boldsymbol{K_v}$ is a positive definite gain matrix. For the purpose of this study we have chosen to directly control the robot's joint velocities about the joint velocities of the model making $\boldsymbol{K_v}$ a diagonal matrix with the diagonal elements set to the control gain K_v.

IV. MODEL SELECTION

Similar to the 1-DOF case, we are constrained to using models with larger inertial forces than the robot indicating $\boldsymbol{M_r} - \boldsymbol{M}$ should be positive definite. Unlike the 1-DOF case however there is now much more freedom to select and shape the model dynamics to get closed loop systems that feel very different to the user.

Realizing that, at least at low-frequencies, the resulting closed loop system will feel like the model to a telerobotic user we have focused on two particular models. The first model, in an effort to minimize the inertia the user feels, tries to make the model match the actual robot as close as possible while still having slightly more mass.

$$\boldsymbol{M_r} = (1+\epsilon)\boldsymbol{M} \quad \text{and} \quad \boldsymbol{C_r} = (1+\epsilon)\boldsymbol{C} \quad \text{for} \quad \epsilon > 0 \tag{22}$$

While the resulting system will have the lowest inertial forces possible, the user will feel the centripetal and Coriolis terms as well as the variation in mass with respect to the robots orientation.

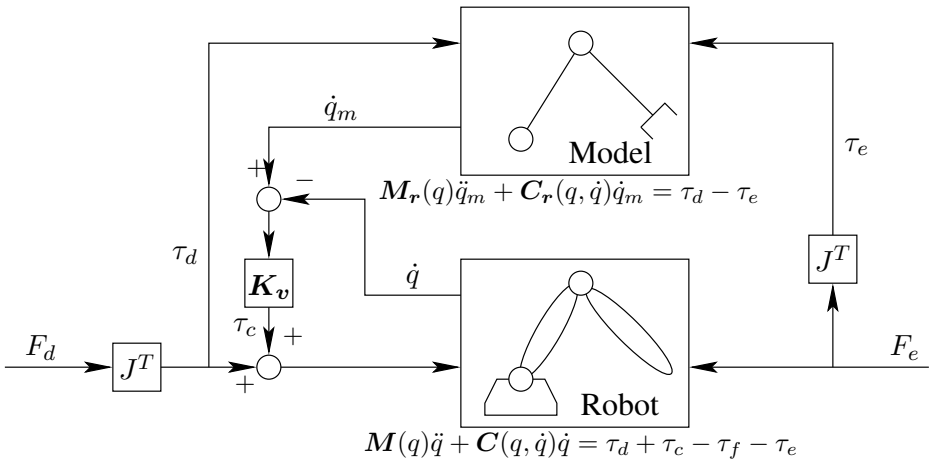

Fig. 4. Multi-DOF model-based force controller.

The second model, in the interest of simplifying the dynamics the user feels, is a point mass model in Cartesian space.

$$M_r \boldsymbol{I}\ddot{x} = F_d - F_e \tag{23}$$

where $\boldsymbol{I}$ is the identity matrix. Converting to joint space and substituting $\dot{x} = J\dot{q}$ and $\ddot{x} = \dot{J}\dot{q} + J\ddot{q}$ this model is equivalent to choosing

$$\boldsymbol{M_r} = M_r J^T J \quad \text{and} \quad \boldsymbol{C_r} = M_r J^T \dot{J} \tag{24}$$

This model can be viewed as having the exact same kinematics as the robot, but with massless links and a point mass at the end-effector.

The trade-off of using a point mass model is the resulting system will only be passive within a reduced portion of the robot's workspace. As the robot approaches singular positions, its effective Cartesian space mass begins to increases drastically while the model Cartesian space mass remains constant by design. Eventually the effective mass of the robot will become greater then M_r in certain directions and the system will no longer be passive.

V. EXPERIMENTAL VALIDATION

To explore how model selection effects the performance of model-based force control and to compare the resulting controllers with more traditional force controllers, we implemented two model-based controllers and a standard proportional force controller on the 2-DOF planar mechanism shown in Fig. 5. The mechanism has $35cm$ long links, and in order to approximate an industrial-like robot, the motors have a gear ratio of $113:1$. The force control algorithms were implemented using a real-time servo loop running at $1kHz$.

We implemented the model-based force controllers using both of the models discussed above. For the matched model case (20) ϵ was set to be 0.01 while $\boldsymbol{M}$ and $\boldsymbol{C}$ where our best estimates of the mass and centripetal/Coriolis matrices of the real robot obtained from a system identification analysis conducted during construction of the robot.

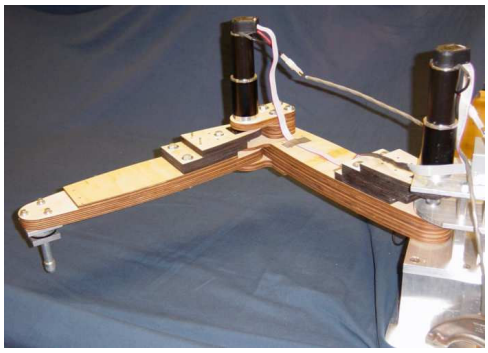

Fig. 5. 2-DOF planar robot used for controller validation.

For the point mass model (24), the model had a uniform mass of $M_r = 5.5kg$ designed to be safely above the maximum effective Cartesian space mass of the robot over the anticipated range of motion. For both models the control gain K_v was set to $30Nms/rad$ which provided good force tracking without excessive sensitivity to the noise in the force sensor.

The proportional force controller was implemented using

$$\tau_a = J^T F_d + J^T \boldsymbol{K_P}(F_d - F_e) \tag{25}$$

where τ_a is the torque applied to the motors. For the experiments shown here, the gain matrix $\boldsymbol{K_p}$ was a diagonal matrix where the two diagonal elements were both set to the same gain K_p to achieve the same control on force error in all directions. The proportional force controller treats both inertial and frictional forces as disturbances which it attempts to reject with a factor of $\frac{1}{1+K_p}$. For the results given below we used two proportional force controllers with K_p values of 1.0 and 2.0 respectively.

A. Telerobotic Force Tracking

The first experiment was designed to compare how the various force controllers would feel to a user of a telerobotic system. A simulated master trajectory was developed where

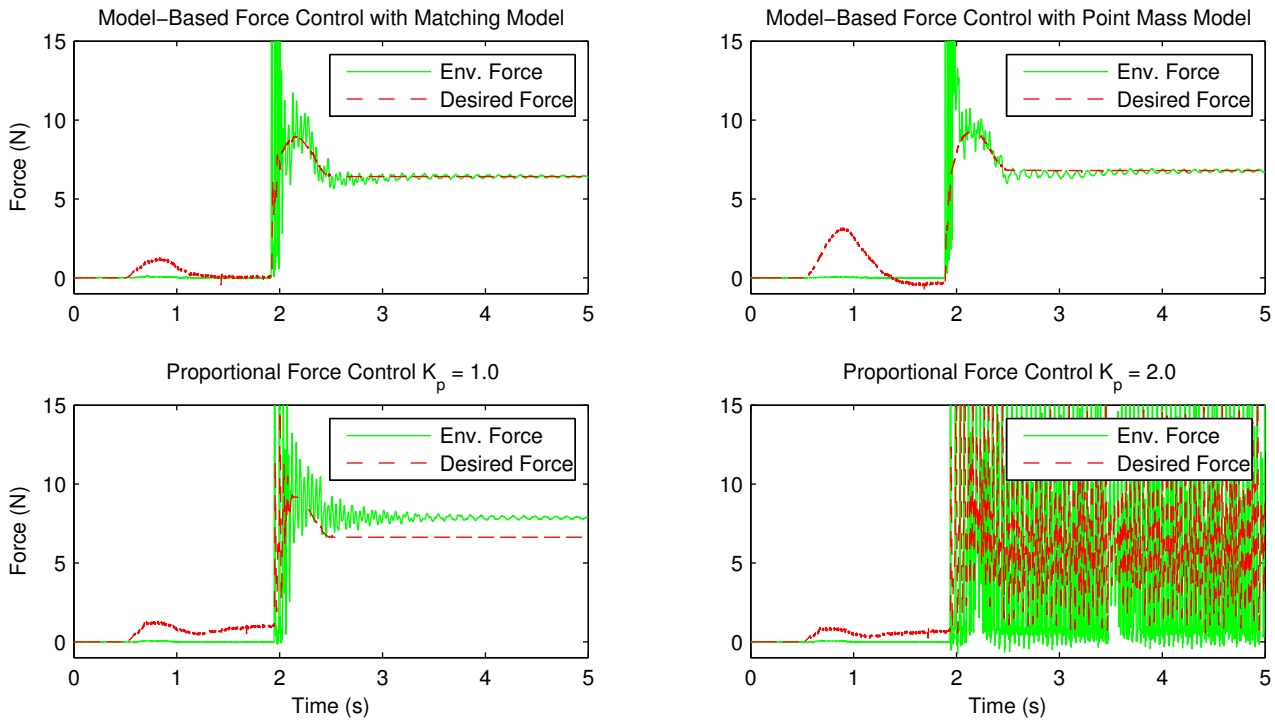

Fig. 6. Desired and measured environmental force responses in the negative x-direction for absolutely stable model-based force controllers (top), and potentially unstable proportional force controllers following a simulated master motion (bottom).

the master accelerated smoothly up to a velocity of $0.20m/s$ in the negative x-direction, maintained this velocity for one second, and then decelerated back to zero velocity by the time the master had traveled $30cm$ in the negative x-direction.

A standard position-position telerobotic controller connected the 2-DOF slave to this simulated master robot using:

$$F_d = k_p(x_{master} - x_{slave}) + k_d(\dot{x}_{master} - \dot{x}_{slave}) \quad (26)$$

where x_{master} is the simulated master position and x_{slave} is the position of 2-DOF robot's end-effector. For this study the control gains were set to $k_p = 100N/m$ and $k_d = 30Ns/m$. Note that in addition to being the desired force provided to the force controllers, F_d also represents the force a human operator would feel at the master device.

After moving approximately $23.5cm$ the slave end-effector impacted an aluminum block mounted rigidly to ground. The impact resulted in a large spike in the measured environment force of about $60N$ for all four force controllers and a position error of about $6.5cm$ corresponding to a steady-state desired force of $F_d \approx 6.5N$.

Fig. 6 gives the desired force and the measured environment force for each force controller in the negative x-direction. As the master begins to accelerate the magnitude of the desired force increases in order to accelerate the 2-DOF robot. This increase in F_d is most pronounced for the point mass model-based controller since it has the largest effective closed-loop mass. The proportional force controllers in contrast are able to hide a portion of the mass at low-frequencies resulting in a smaller F_d in this acceleration regime.

Since the two model-based force controllers completely cancel out friction, F_d goes to zero once both master and slave reach a steady-state velocity. The proportional controllers on the other hand do not reject friction completely and F_d settles to a constant value representing the remaining friction forces a user would feel when moving the robot in free-space.

Upon impacting the aluminum block the proportional force controller with $K_p = 2$ is clearly unstable. The large spikes in the measured force response represent the robot continuously bouncing off the aluminum block in a persistent limit-cycle while the spikes in F_d represent the damping in the position-position controller. Reducing the proportional control gain to $K_p = 1$ stabilizes the system although the relatively small control gain results in a significant steady-state force error of about 20%.

The two model-based force controllers on the other hand achieve perfect steady-state force tracking once the transients excited by impact settle down. Note the small oscillations in the force measurement that exist well past the moment of impact in all three stable controllers are caused by long-lasting vibrations in the table that both the robot and the aluminum block are mounted on.

B. *Effects of Nonlinear Dynamics*

The second test presented here was designed to show the ability of the point mass model-based force controller to

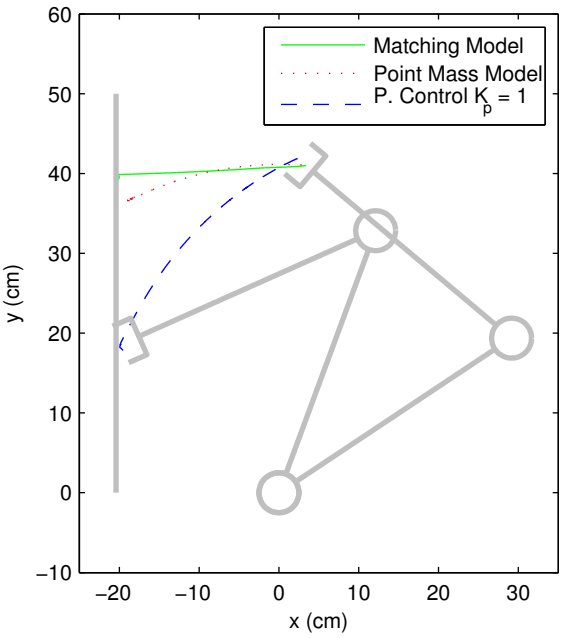

Fig. 7. Position trajectories in response to a unit force command in the negative x-direction for model-based force controllers and proportional force controller with $K_p = 1$.

effectively linearize the dynamics of the robot. Instead of tracking a master device as before, the three stable controllers from above were given a desired force of $F_d = 1$ in the negative x-direction. Fig. 7 gives the resulting trajectories as the robot moves approximately $20cm$ in the negative x-direction and impacts the same aluminum block from before along with the start and end configuration for the robot when using the matching model controller.

In order to achieve the lightest possible model-based controller and to maintain passivity over the entire workspace the model-based controller using the matching model makes no attempt to hide the centripetal and Coriolis forces. Quite on the contrary, by effectively removing the friction forces the centripetal and Coriolis forces, despite being small, can now significantly effect the motion of the robot. As the robot begins to accelerate in response to the desired force F_d the centripetal and Coriolis forces grow resulting in significant motion in the y-direction.

The controller using the point mass model on the other hand trades a larger effective mass and a limited workspace over which the robot is passive in exchange for linearized dynamics. As expected for a linear system, when the desired force is applied to the point mass controller the resulting motion is almost perfectly aligned with the desired force vector.

The proportional controller in comparison falls somewhere between the two extremes. Hiding half the inertial forces, which include the centripetal and Coriolis forces, and half the friction, the trajectory followed by the proportional force controller is mostly aligned with the desired force vector although there is still motion in the y-direction.

VI. CONCLUSIONS

In designing model-based force control our primary objective was to produce a force controller for slave devices in telerobotic systems that would both precisely control contact forces and maintain safe and stable operation in all situations. The passivity framework has both provided a means to explain instability observed in traditional force controllers and a method to test our designs for the desired level of robustness.

In 1-DOF, passivity analysis has shown model-based force control to be stable when interacting with all environments. Furthermore, having been designed for passivity, model-based force control has also proven extremely robust to such typical non-idealities as unmodeled dynamics and non-linear friction forces.

The experimental results of this paper show that this extreme robustness of the model-based force control extends into multi-DOF implementations. Furthermore, in multiple degree of freedom systems the model reference force control adds an additional and unique level of flexibility in controlling the closed loop dynamics of the robot. For example, a point mass model effectively linearized the dynamics of the robot at the cost of a larger effective mass and a reduced workspace over which the system is passive. This design freedom allows the control designer to more carefully determine how the resulting telerobotic system will feel to the user without worrying about pushing the stability boundary.

REFERENCES

[1] W. S. Kim, B. Hannaford, and A. K. Bejczy, "Force-reflection and shared compliant control in operating telemanipulators with time delay," *IEEE Trans. Robot. Automat.*, vol. 8, no. 2, pp. 176–185, 1992.

[2] M. Mahvash and A. M. Okamura, "Friction compensation for a force-feedback telerobotic system," in *IEEE International Conference on Robotics and Automation*, May 2006, pp. 3268–3273.

[3] R. W. Daniel and P. McAree, "Fundamental limits of performance for force reflecting teleoperators," *International Journal of Robotics Research*, vol. 17, no. 8, pp. 811–830, 1998.

[4] K. Hashtrudi-Zaad and S. E. Salcudean, "Transparency in time-delayed systems and the effect of local force feedback for transparent teleoperation," *IEEE Trans. Robot. Automat.*, vol. 18, no. 1, pp. 108–114, 2002.

[5] J. Park and O. Khatib, "A haptic teleoperation approach based on contact force control," *International Journal of Robotics Research*, vol. 25, no. 5-6, pp. 575–591, 2006.

[6] E. Colgate and N. Hogan, "An analysis of contact instability in terms of passive physical equivalents," in *IEEE International Conference on Robotics and Automation*, May 1989, pp. 404–409.

[7] W. S. Newman, "Stability and performance limits of interaction controllers," *Journal of Dynamic Systems, Measurement, and Control-Transactions of the ASME*, vol. 114, no. 4, pp. 563–570, 1992.

[8] W. S. Newman and Y. Zhang, "Stable interaction control and coulomb friction compensation using natural admittance control," *Journal of Robotic Systems*, vol. 11, no. 1, pp. 3–11, 1994.

[9] J. S. Hart and G. Niemeyer, "Model-reference based wave-variable force control," in *IEEE International Conference on Robotics and Automation*, May 2009, pp. 4074–4079.